Vesicular trafficking through cortical actin during exocytosis is regulated by the Rab27a effector JFC1/Slp1 and the RhoA-GTPase–activating protein Gem-interacting protein

Jennifer L. Johnson[a], Jlenia Monfregola[a], Gennaro Napolitano[a], William B. Kiosses[b], and Sergio D. Catz[a]
[a]Department of Molecular and Experimental Medicine and [b]Core Microscopy Facility, Scripps Research Institute, La Jolla, CA 92037

ABSTRACT Cytoskeleton remodeling is important for the regulation of vesicular transport associated with exocytosis, but a direct association between granular secretory proteins and actin-remodeling molecules has not been shown, and this mechanism remains obscure. Using a proteomic approach, we identified the RhoA-GTPase–activating protein Gem-interacting protein (GMIP) as a factor that associates with the Rab27a effector JFC1 and modulates vesicular transport and exocytosis. GMIP down-regulation induced RhoA activation and actin polymerization. Importantly, GMIP-down-regulated cells showed impaired vesicular transport and exocytosis, while inhibition of the RhoA-signaling pathway induced actin depolymerization and facilitated exocytosis. We show that RhoA activity polarizes around JFC1-containing secretory granules, suggesting that it may control directionality of granule movement. Using quantitative live-cell microscopy, we show that JFC1-containing secretory organelles move in areas near the plasma membrane deprived of polymerized actin and that dynamic vesicles maintain an actin-free environment in their surroundings. Supporting a role for JFC1 in RhoA inactivation and actin remodeling during exocytosis, JFC1 knockout neutrophils showed increased RhoA activity, and azurophilic granules were unable to traverse cortical actin in cells lacking JFC1. We propose that during exocytosis, actin depolymerization commences near the secretory organelle, not the plasma membrane, and that secretory granules use a JFC1- and GMIP-dependent molecular mechanism to traverse cortical actin.

Monitoring Editor
Julie Brill
The Hospital for Sick Children

Received: Dec 8, 2011
Revised: Feb 29, 2012
Accepted: Mar 16, 2012

This article was published online ahead of print in MBoC in Press (http://www.molbiolcell.org/cgi/doi/10.1091/mbc.E11-12-1001) on March 21, 2012.

Address correspondence to: Sergio D. Catz (scatz@scripps.edu).

Abbreviations used: BM-PMN, bone marrow–derived polymorphonuclear neutrophil; DAPI, 4′, 6-diamidino-2-phenylindole, dihydrochloride; DMSO, dimethyl sulfoxide; ECFP, enhanced cyan fluorescent protein; ELISA, enzyme-linked immunosorbent assay; FITC, fluorescein isothiocyanate; fMLF, formyl-methionyl-leucyl-phenylalanine; FRET, fluorescence resonance energy transfer; GFP, green fluorescent protein; GMIP, Gem-interacting protein; GST, glutathione *S*-transferase; HPLC, high-performance liquid chromatography; IgG, immunoglobulin G; JFC1, synaptotagmin-like protein 1 [Slp1]; JFC1-KO, JFC1 knockout; KOMP, Knockout Mouse Project; LAMP3, lysosome-associated membrane protein 3; LPS, lipopolysaccharide; MPO, myeloperoxidase; MS/MS, tandem mass spectrometry; PBS, phosphate-buffered saline; PE, phycoerythrin; PMA, phorbol, 12-myristate, 13-acetate; RBD, RhoA-binding domain; RhoA-GAP, RhoA GTPase–activating protein; ROCK, RhoA-associated kinase; RPMI, Roswell Park Memorial Institute; siRNA, small interfering RNA; SLO, streptolysin O; TIRFM, total internal reflection fluorescence microscopy; YFP, yellow fluorescent protein.

INTRODUCTION

Regulated exocytosis is an essential process that controls the release of proteins stored in secretory organelles into the extracellular milieu. Although secretory cargo proteins are usually specific for particular cellular systems, the process of exocytosis is relatively conserved in eukaryotic cells. Regulated secretion involves the transport of cargoes from the intracellular site of storage to the plasma membrane through the cytoskeleton, followed by vesicle docking, fusion of the vesicular membrane with the plasmalemma, and cargo release. The efficiency and specificity of vesicular transport relies on Rab proteins, which are Ras-like small GTPases, and on their specific effectors (Pfeffer, 2001). In particular, Rab27a and its effectors JFC1 and Munc13-4 are master regulators of exocytosis that are expressed in both hematopoietic and nonhematopoietic cells (McAdara-Berkowitz *et al*., 2001; Feldmann *et al*., 2003; Tolmachova *et al*., 2004; Neeft *et al*., 2005; Brzezinska *et al*., 2008). Deficiencies in Rab27a or its effector molecules are associated with human immunodeficiencies due to malfunction of cytotoxic T-lymphocytes, natural killer cells,

and neutrophils (Stinchcombe *et al.*, 2001; Munafo *et al.*, 2007; Holt *et al.*, 2008; Brzezinska *et al.*, 2008; Wood *et al.*, 2009). Furthermore, GTPases of the Rab27 family and their effectors have been associated with the development of metabolic diseases (Yi *et al.*, 2002) and cancer (Catz, 2008; Wang *et al.*, 2008; Hendrix *et al.*, 2010). Despite the biological and medical importance of the process of exocytosis, the molecular mechanisms underlying regulated secretion and the molecular components of the secretory machinery are incompletely characterized.

Neutrophil exocytosis is a crucial event in inflammation and host defense. These granulocytes contain four types of secretory organelles that hold a variety of specialized proteins essential for the regulation of the innate immune response. Tight regulation of the exocytic process is necessary, because unrestricted release of the toxic content of neutrophil granules is injurious to the host. In this regard, the secretory proteins stored in azurophilic granules play a fundamental role in the damage to endothelium associated with endotoxemia and sepsis (Clark *et al.*, 2007; Brovkovych *et al.*, 2008). Thus exocytosis in neutrophils is important for modulating the level of secretory factors present in inflammatory foci and their deleterious consequences; the analysis of the molecular mechanisms regulating exocytosis therefore has important biological significance.

There is increasing evidence that secretory granules are in constant movement in the plane parallel to the plasma membrane andthat vesicular dynamics are an important factor in efficient engagement of granules in exocytosis, increasing the probability of interactions with docking domains at the plasma membrane (Degtyar *et al.*, 2007; Brzezinska *et al.*, 2008; Johnson *et al.*, 2010b). In granulocytes, JFC1 and Rab27a colocalize at highly dynamic secretory organelles and play an important role in the regulation of the vesicular dynamic processes that precede azurophilic granule exocytosis (Munafo *et al.*, 2007; Brzezinska *et al.*, 2008). While in some cellular systems the actin cytoskeleton regulates vesicular movement during exocytosis (Manneville *et al.*, 2003), it has been proposed that the actin cytoskeleton in neutrophils limits the rate and extent of exocytosis by controlling the access of neutrophil granules to the plasma membrane (Jog *et al.*, 2007). Other studies have presented evidence of a dual role for actin in exocytosis and suggested the actin cytoskeleton has both direct inhibitory and facilitatory roles in regulated secretion in nonexcitable cells (Muallem *et al.*, 1995; Lang *et al.*, 2000). Despite these observations, the mechanisms underlying granule dynamics in relationship to modification in the actin network are unclear, and the molecular components that regulate such mechanisms are currently unknown.

The Rab27a effector JFC1 (synaptotagmin-like protein 1 [Slp1]) was originally isolated from leukocytes and is widely expressed in tissues with a secretory function (McAdara-Berkowitz *et al.*, 2001). JFC1, a 562-amino-acid-long protein, contains an amino-terminal Rab-binding domain and tandem C2-domains in its carboxy-terminus (McAdara-Berkowitz *et al.*, 2001; Catz *et al.*, 2002). In granulocytes, endogenous JFC1 colocalizes with Rab27a at the azurophilic granule membrane (Munafo *et al.*, 2007). JFC1 directly binds to Rab27a (Fukuda, 2002; Strom *et al.*, 2002), and together they regulate azurophilic granule dynamics and exocytosis in granulocytes (Brzezinska *et al.*, 2008) and secretion of prostate-specific antigen in prostate carcinoma cells (Catz, 2008). Owing to its ability to bind to Rab27a through its amino-terminal domain and to plasma membrane–associated phosphoinositides through its C2A domain, JFC1 was postulated to regulate vesicular tethering or docking (Catz *et al.*, 2002). A second C2 domain, C2B, stretches between residues 398 and 534 of the JFC1 molecule (McAdara-Berkowitz *et al.*, 2001). The C2B domain of JFC1 is not well characterized, and its putative molecular interactions remain unknown.

In this work, we have identified the RhoA GTPase-activating protein (RhoA-GAP) GMIP (Gem-interacting protein) as a JFC1-C2B domain–interacting protein. GMIP carries a Rho-GAP activity that acts specifically on RhoA, but not on Rac or Cdc42 (Aresta *et al.*, 2002), and mediates an inhibitory effect on actin polymerization through the GMIP-RhoA-GAP domain (Aresta *et al.*, 2002). Given the association between actin remodeling and exocytosis, the interaction between JFC1 and GMIP is highly significant. In this paper, we present the characterization of a mechanism of cross-talk between the granule secretory components and actin-remodeling molecules and have established roles for the Rab27a effector JFC1 and the RhoA-GAP GMIP in the control of vesicular dynamics and azurophilic granule exocytosis in association with the regulation of the actin network.

RESULTS

RhoA-GAP GMIP associates with the secretory factor JFC1

To better understand the mechanism mediated by JFC1 in the regulation of vesicular transport associated with cargo release, we searched for regulatory proteins that interact with JFC1. Using a proteomic approach consisting of the immunoprecipitation of endogenous JFC1 from human neutrophils followed by mass spectrometry analysis of the pulled-down proteins from a selected band, we identified the RhoA GTPase-activating protein GMIP (Figure 1A). In the same sample, we also identified a serine/threonine kinase, whose specific interaction with JFC1 is being validated by other methods in our laboratory. Because of its ability to mediate cytoskeleton remodeling (Aresta *et al.*, 2002; Hatzoglou *et al.*, 2007), its high expression in tissues and cells with secretory function (including leukocytes; Aresta *et al.*, 2002), and its association with JFC1, GMIP was selected as a possible candidate for regulation of JFC1-dependent exocytosis. To confirm expression of GMIP in granulocytes, we developed a polyclonal antibody directed at residues 13–26 of GMIP that recognizes both the human and mouse isoforms. As shown in Figure 1B, this antibody identifies a single band at ~108 kDa in neutrophils, the predicted molecular weight of GMIP. Importantly, GMIP, which is weakly expressed in promyelocytic cells, is strongly up-regulated upon myeloid differentiation to granulocytic or macrophage lineages (Figure 1C). This mimics the results obtained for JFC1 and Rab27a expression during myeloid differentiation (Figure 1C and Munafo *et al.*, 2007, respectively), further supporting a role for these proteins in the regulation of the secretory pathway in myeloid cells. To confirm that GMIP specifically associates with JFC1 and to identify the domains of JFC1 involved in this interaction, we utilized a pulldown assay using agarose-bound glutathione *S*-transferase (GST)-JFC1 fusion proteins to pull down GMIP from neutrophil lysates under stringent conditions. Our results show that GMIP associates with full-length JFC1 but not with GST, empty beads, or with the amino-terminus of JFC1 containing the Rab27a-binding domain (Figure 1D). Importantly, GMIP specifically interacted with the C2B domain of JFC1 but not with its C2A domain and therefore constitutes the first molecule identified so far to associate with the C2B domain of JFC1.

Western blot analysis of neutrophil subcellular fractionations indicated that GMIP separates between a soluble (cytosolic form) and a membrane-associated fraction (Figure 1E). In membranes separated using sucrose gradients, GMIP cofractionated with RhoA, as well as with the secretory protein JFC1. GMIP also cofractionates with a membrane fraction containing low-density, myeloperoxidase (MPO)-positive granules. This is in agreement with previous studies

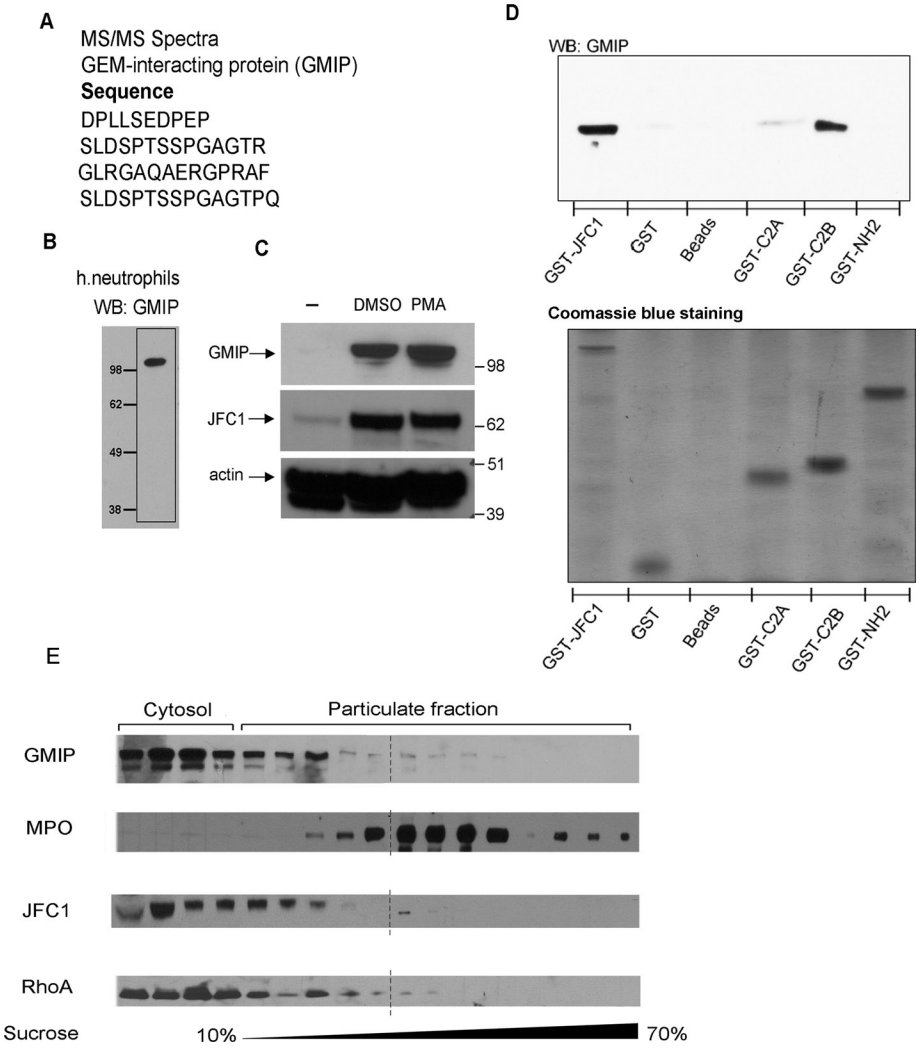

FIGURE 1: The RhoA-GAP GMIP associates with JFC1 in neutrophils. (A) Endogenous JFC1 was immunoprecipitated from human neutrophils and the proteins that were pulled down with JFC1 were analyzed by MS/MS. The peptides corresponding to GMIP identified by MS/MS are shown. (B) Expression of GMIP in human neutrophils. Proteins from 5×10^6 cell equivalents were resolved by gel electrophoresis and GMIP was detected by Western blotting using an antibody against the amino-terminal domain of GMIP. (C) Western blot analysis of the expression of GMIP and JFC1 in human promyelocytic HL-60 cells during differentiation to granulocyte (DMSO) or monocytes/macrophage (PMA) lineages. (D) The association between JFC1 and GMIP was analyzed in pulldown assays using recombinant GST full-length JFC1 or the C2A, C2B, or amino-terminal (-NH2) domains of JFC1 to pull down endogenous GMIP from human neutrophil lysates. Equal input protein was analyzed by Coomassie Blue staining. (E) GMIP, JFC1, and RhoA cofractionate with each other and with a subset of MPO-containing granules. Protein expression in human neutrophil subcellular fractions was analyzed by Western blotting. Results are representative of three experiments performed with independent donors.

showing that the secretory factors Rab27a, JFC1, and Munc13-4 cofractionate with a subpopulation of low-density granules that constitute the exocytosable pool of azurophilic granules (Munafo *et al.*, 2007) but not with high-density azurophilic granules that represent the nonexocytosable pool (Brzezinska *et al.*, 2008; Johnson *et al.*, 2010a).

GMIP regulates RhoA activity and actin polymerization

It has been proposed that GMIP mediates RhoA inactivation through its RhoA-GAP activity (Aresta *et al.*, 2002; Hatzoglou *et al.*, 2007). To analyze whether GMIP has RhoA-inhibitory activity in phagocytes, we measured RhoA activity in GMIP-down-regulated, living HL-60 cells using a well-characterized fluorescence biosensor that preserves reversible membrane interactions (Pertz *et al.*, 2006). To down-regulate GMIP in HL-60 cells, we used small interfering RNA (siRNA) oligonucleotides that significantly and specifically down-regulated GMIP expression without affecting JFC1 expression (Figure 2A). Next, using the RhoA biosensor, we showed that GMIP-down-regulated HL-60 cells have significantly higher constitutive levels of active RhoA than control cells (Figure 2, B and C). The RhoA-GAP activity of GMIP was further demonstrated using a well-established pulldown assay in GMIP-down-regulated 293T cells (Supplemental Figure S1). Our results are in agreement with previous reports identifying GMIP as a specific RhoA GAP (Aresta *et al.*, 2002; Hatzoglou *et al.*, 2007). To determine whether decreased GMIP expression and high RhoA activity correlate with high actin polymerization, we transfected GMIP-down-regulated granulocytes with the expression vector yellow fluorescent protein (YFP)-actin and followed actin remodeling in living cells by using total internal reflection fluorescence microscopy (TIRFM), a method that allows real-time measurements of actin polymerization (Kuhn and Pollard, 2005). Our results, presented in Figure 2, D and E, show that GMIP-down-regulated cells have significantly increased levels of actin polymerization, as demonstrated by an increase in the length of the actin protrusions, thus establishing a direct role for GMIP in actin remodeling in phagocytes.

GMIP regulates vesicular transport in granulocytes

Because vesicular trafficking depends on actin remodeling and is directly linked to the secretory pathway (Muallem *et al.*, 1995; Lang *et al.*, 2000), and GMIP regulates actin polymerization, we next asked whether GMIP regulates vesicular transport. To analyze this, we studied azurophilic granule dynamics in GMIP-down-regulated cells using TIRFM. In these experiments, we utilized GMIP-down-regulated cells expressing the azurophilic granule marker lysosome-associated membrane protein 3 (LAMP3) as a green fluorescent protein (GFP) fusion protein (Figure 3A and Supplemental Movies S1 and S2) and followed vesicle dynamics using a quantitative microscopy approach as described previously by our group (Johnson *et al.*, 2010b). We found that GMIP-down-regulated cells have a significant decrease in the number of granules undergoing fast movement (LAMP3 granules with speed > 0.13 μm/s, siRNA control vs. siRNA GMIP, $p < 0.03$; Figure 3B) and an increase in the number of granules with slow or no motility (LAMP3 granules with speed < 0.04 μm/s, siRNA control vs. siRNA GMIP, $p < 0.04$; Figure 3B). However, no significant differences were observed in the number of azurophilic granules

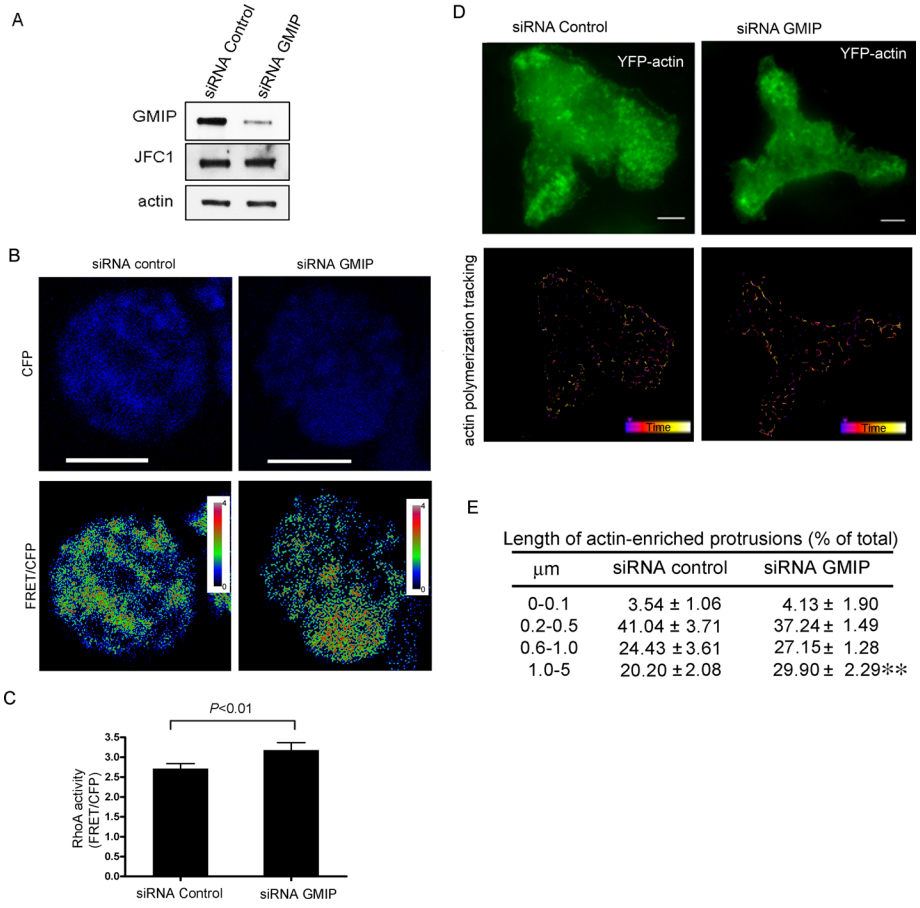

FIGURE 2: GMIP-down-regulated cells have increased RhoA activity and increased levels of actin polymerization. (A) Down-regulation of GMIP expression in HL-60 granulocytes using siRNA. HL-60 cells were transfected by nucleofection with GMIP-specific or control (nonsilencing) siRNAs as described in *Materials and Methods*. The cells were differentiated to granulocytes and analyzed for the expression of GMIP and JFC1 by Western blotting. (B) HL-60 cells were down-regulated for GMIP expression and transfected with a RhoA biosensor that detects the intramolecular interaction between YFP-RhoA-GTP and the CFP-RhoA–binding domain of Rhotekin, which only recognizes the GTP-bound (active form) of RhoA. Increased RhoA activity is detected as an increment in FRET signal. FRET images are pseudocolored, with the color indicating the relative value at each pixel. (C) Quantification of RhoA activity using the RhoA biosensor. n = 42 control cells and 35 GMIP-down-regulated cells from two independent experiments. Statistical analysis was performed using the nonparametric Mann-Whitney test. (D and E) GMIP-down-regulated HL-60 cells were transfected with YFP-actin, and the dynamics of actin polymerization were analyzed by TIRFM. The length of actin-enriched protrusions was measured using an integrated algorithm for the analysis of continuous particle tracking (Imaris 7.0; Bitplane Scientific Software, South Windsor, CT). Analysis of actin dynamics was followed for 1 min. (D) representative images of YFP-actin expression and tracking. (E) The differences in actin protrusion lengths between control and GMIP-down-regulated cells from three independent experiments were analyzed using the Mann-Whitney test. **, $p < 0.005$.

distributed in close proximity to the plasma membrane (the exocytic active zone) between GMIP-down-regulated and control cells (Figure 3C), indicating that GMIP down-regulation induces granule transition from a high-speed to a low-motility pool of granules, rather than interfering with the distribution of a particular set of granules.

GMIP regulates exocytosis

Next, to directly analyze whether GMIP regulates exocytosis, we down-regulated GMIP expression in granulocytes and subsequently used these cells in secretion experiments. Similar to JFC1-down-regulated cells (Brzezinska *et al.*, 2008), GMIP-down-regulated cells showed impaired MPO secretion (Figure 4A). However, the impaired exocytosis shown by GMIP-deficient cells was overcome by preincubation of cells with cytochalasin D, an agent that induces actin depolymerization and facilitates exocytosis in granulocytes (Figure 4A). To analyze whether GMIP also plays a significant role in exocytosis in primary neutrophils, we then performed secretion assays in mouse and human neutrophils in which GMIP function was inhibited through molecular interference by introducing specific antibodies directed at the amino-terminal domain of GMIP in streptolysin O (SLO)-permeabilized cells. This approach has been utilized previously to demonstrate the participation of the Rab27a/b effector Myrip/Slac-c2 in amylase release in parotid acinar cells (Imai *et al.*, 2004) and of JFC1 in azurophilic granule exocytosis in human neutrophils (Brzezinska *et al.*, 2008). Further supporting this approach, previous studies showed that SLO-permeabilized neutrophils undergo exocytosis in the presence of GTP analogues and Ca^{2+}, that the efficiency of the exocytic process in SLO-permeabilized neutrophils is functionally coupled to the formyl-methionyl-leucyl-phenylalanine (fMLF) receptor (Cockcroft, 1991), and that the ultrastructure of neutrophils is largely preserved in SLO-permeabilized neutrophils (Brown *et al.*, 2003). Importantly, our results show that interference with GMIP function impairs azurophilic granule exocytosis in both murine and human neutrophils (Figure 4, B and C, respectively). Altogether, our observations using HL-60 cells and primary neutrophils strongly support a role for the RhoA-GAP GMIP in regulated secretion.

Inactivation of the RhoA-signaling pathway induces actin depolymerization and enhances exocytosis

To analyze a possible role for RhoA-dependent signaling in granulocyte exocytosis, we first examined whether RhoA is recruited to azurophilic granules in neutrophils. To this end, we performed immunofluorescence analysis of endogenous proteins and determined by its colocalization with the azurophilic granule markers elastase and myeloperoxidase that RhoA localizes at azurophilic granules (Figure 5A). The observation that only a subpopulation of azurophilic granules show colocalization with RhoA correlates with previous reports that only ~20% of azurophilic granules are able to engage in exocytosis which is also in agreement with the percentage of azurophilic granules in a given neutrophil expressing the secretory proteins Rab27a and JFC1 (Johnson *et al.*, 2010a). Next, to evaluate the distribution of RhoA activity in relationship to the secretory protein JFC1, we cotransfected granulocytes with the expression vector DsRed-JFC1 and with a RhoA biosensor and analyzed live cells by using fluorescence resonance energy transfer (FRET) microscopy. We found that RhoA colocalizes with JFC1-positive

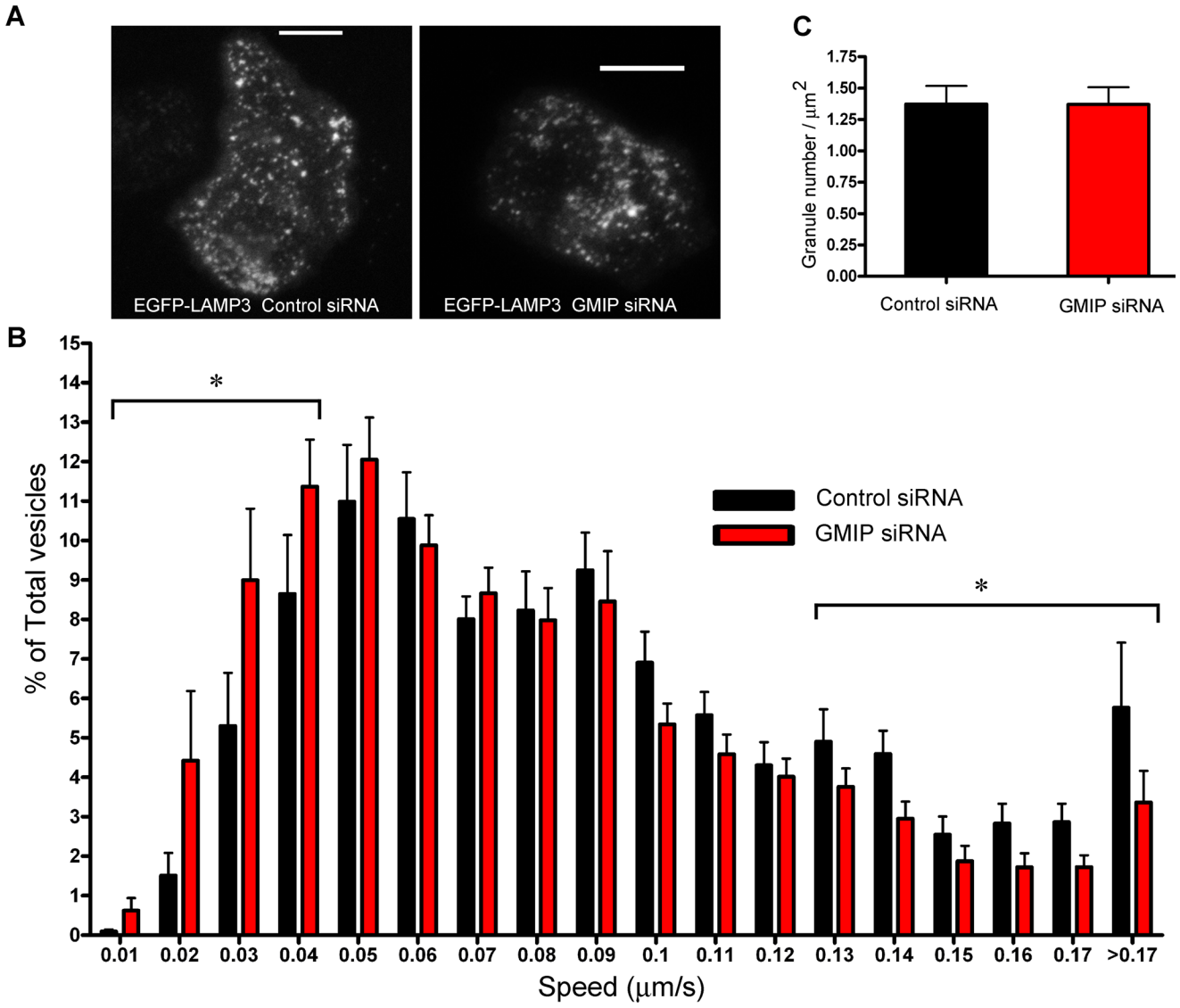

FIGURE 3: Vesicular trafficking is impaired in GMIP-down-regulated cells. Control and GMIP-down-regulated cells were transfected with the expression vector for the azurophilic granule marker LAMP3 (CD63, EGFP-LAMP3) and analyzed by TIRFM as described in *Materials and Methods*. (A) Representative images from GMIP-down-regulated or control cells expressing EGFP-LAMP3. Scale bar: 5 µm. A complete sequence can be observed in associated Movies S1 and S2. (B) Histograms of the speeds of LAMP3-expressing granules from GMIP-down-regulated or control cells. Images were acquired at 1-s intervals for 2 min with 300 ms of exposure time and analyzed using Imaris 7.0 (Bitplane Scientific Software). Granule speeds were binned in 0.01-µm/s increments and plotted as a percentage of total granules for a given cell. A total of 4164 and 4994 vesicles from 22 control and 25 GMIP-down-regulated cells were analyzed in three independent experiments. Data are expressed as mean ± SEM. The number of highly motile granules (speed > 0.13 µm/s) was significantly decreased in GMIP-down-regulated cells (*, $p < 0.03$). Also, the number of granules with slow or no motility (speed < 0.04 µm/s) was significantly increased in cells lacking GMIP (*, $p < 0.04$). Statistical analysis was performed using unpaired *t* test. (C) Quantitative analysis of the number of azurophilic granules identified in the TIRFM zone per adherent membrane area unit for control or GMIP-deficient cells is shown.

granules. Interestingly, RhoA activity was detected in surrounding areas of JFC1-expressing granules and showed a polarized distribution on a subpopulation of these granules (Figure 5B). To evaluate whether the RhoA downstream signaling pathway is associated with the regulation of actin remodeling in granulocytes, we then inhibited RhoA-associated kinase (ROCK) activity pharmacologically and found that polymerization of cortical actin is down-regulated by treatment with the ROCK inhibitor (Figure 5C). Next we reasoned that if GMIP regulates vesicular trafficking and exocytosis by down-regulation of RhoA, inactivation of RhoA-dependent pathways should enhance exocytosis. To analyze this, and since Rho inhibitors are not isomer-specific, we used the ROCK inhibitor Y27632 and measured azurophilic granule exocytosis in human neutrophils. The results of these secretion experiments confirmed that inhibition of RhoA downstream effectors enhance exocytosis in neutrophils (Figure 5D). Altogether, these results suggest that RhoA-dependent signaling around secretory granules is inhibitory for granulocyte secretion. Finally, to correlate these results with a possible role of GMIP in RhoA regulation at secretory granules, we analyzed RhoA activity by using the RhoA biosensor in GMIP-deficient cells expressing

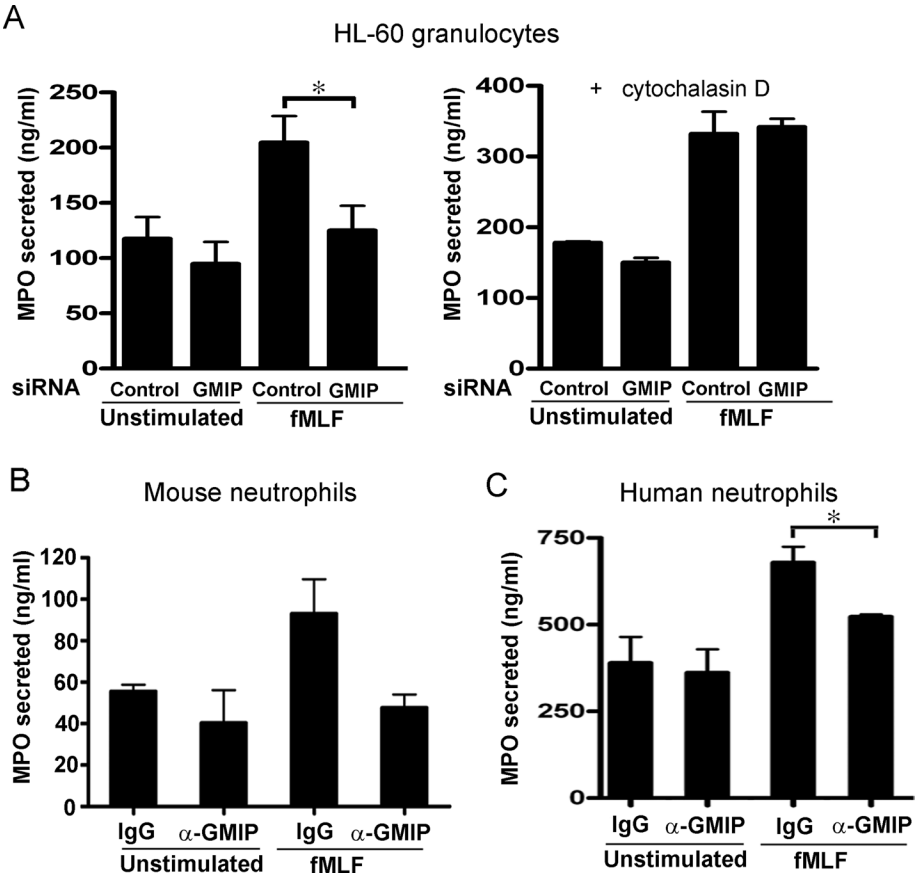

FIGURE 4: GMIP regulates azurophilic granule exocytosis. (A) HL-60 cells were transfected with GMIP-specific siRNA or with control nonsilencing siRNA and differentiated as described in the text. The cells were harvested, washed with PBS, and stimulated with fMLF (1 μM) for 10 min (left panel). Where indicated, the cells were treated with cytochalasin D (10 μg/ml) for 10 min before addition of fMLF (right panel). The cells were spun down, and the concentration of MPO in the supernatants was determined by ELISA. Results are the mean ± SEM of three independent experiments. (B and C) Interference with GMIP inhibits MPO secretion in permeabilized neutrophils. MPO exocytosis was evaluated in SLO-permeabilized neutrophils after incubation with anti-GMIP rabbit polyclonal antibodies or control IgG obtained from pre-bleeds of the rabbit. The cells were treated with 100 ng/ml LPS and stimulated with 1 μm fMLF. Results represent the mean ± SEM from two (B) or four (C) independent experiments. *, $p < 0.05$.

DsRED-JFC1. We found that RhoA activity increases around JFC1-expressing granules in cells deficient for GMIP expression (Figure 5E), further supporting a role for this RhoA-GAP in the regulation of RhoA at the granule-surrounding areas.

Secretory organelles move in areas deprived of polymerized actin

The experiments described in the preceding section suggested an inverse correlation between actin polymerization and exocytosis. To determine a possible association between secretory organelle movement and actin remodeling, we analyzed the dynamics of JFC1-expressing granules in relationship to actin remodeling at the exocytic active zone in live cells. To this end, we coexpressed DsRed-JFC1 and EYFP-actin in HL-60 cells and analyzed their subcellular distribution using TIRFM. We chose TIRFM because this technique favors the observation of secretory organelle dynamics at the exocytic active zone (Brzezinska *et al.*, 2008; Johnson *et al.*, 2010b) and allows the analysis of actin polymerization in the proximity of the plasma membrane, while abolishing the contribution of background fluorescence from nonpolymerized soluble cytoplasmic actin (Bretschneider *et al.*, 2004). Importantly, the expression of actin fluorescent chimeras does not interfere with cell movement, cell–cell contact, or formation of polarized cells (Ehrlich *et al.*, 2002; Hoppe and Swanson, 2004). In TIRFM, YFP-actin is visualized as localized foci of actin polymerization in the cell body or as dynamic actin protrusions in the periphery, depending on the perpendicular or parallel position of the filament in relation to the coverslip. Importantly, JFC1-containing vesicles were only observed in areas near the plasma membrane lacking foci of polymerized actin (Figure 6A). Furthermore, a halo lacking polymerized actin was always visualized around secretory vesicles (Figure 6A, lower panels), suggesting that secretory granules that are distributed at the exocytic active zone are able to maintain an actin-free environment in their surrounding areas. Next, to establish a correlation between granule movement and actin polymerization, we analyzed the dynamics of JFC1-expressing granules in association with actin remodeling in live cells treated with cytochalasin D, an actin-depolymerizing agent that increases the secretory response to physiological stimuli (Jog *et al.*, 2007). We showed that in untreated cells, which are characterized by a highly dynamic mechanism of actin remodeling at the interface with the plasma membrane, only the areas with low actin-remodeling activity were populated with motile secretory granules (Figure 6, B and C; see also Figure 6B, inset, and Movie S3). Cytochalasin D treatment completely abolished actin remodeling but did not prevent granule movement (Figure 6, B and C; see also Movie S4), although it caused a shift in granule speed, with treated cells showing increased numbers of JFC1-positive secretory organelles moving at lower speed (Figure 6D). Furthermore, abrogation of actin polymerization did not significantly affect granule displacement (Figure 6E). In contrast with the mild effect of cytochalasin D on granule dynamics, treatment with cytochalasin D significantly increased the number of JFC1-positive secretory organelles at the exocytic active zone (Figure 6, F and G). These granules are exocytosis-competent, since stimulation of cytochalasin D–treated cells significantly amplifies exocytosis (Figure 6H). Altogether, our data suggest that JFC1-containing granules exclude polymerized actin from the areas surrounding the vesicle and that actin remodeling is not necessary for granule dynamics in the plane parallel to the plasma membrane (the exocytic active zone), but instead actin depolymerization facilitates granule access to the exocytic active zone and favors exocytosis.

JFC1 regulates RhoA activity and vesicular transport through the actin cortex to facilitate exocytosis

To analyze a possible role of JFC1 in the regulation of RhoA, we transfected primary neutrophils from wild-type and JFC1-knockout

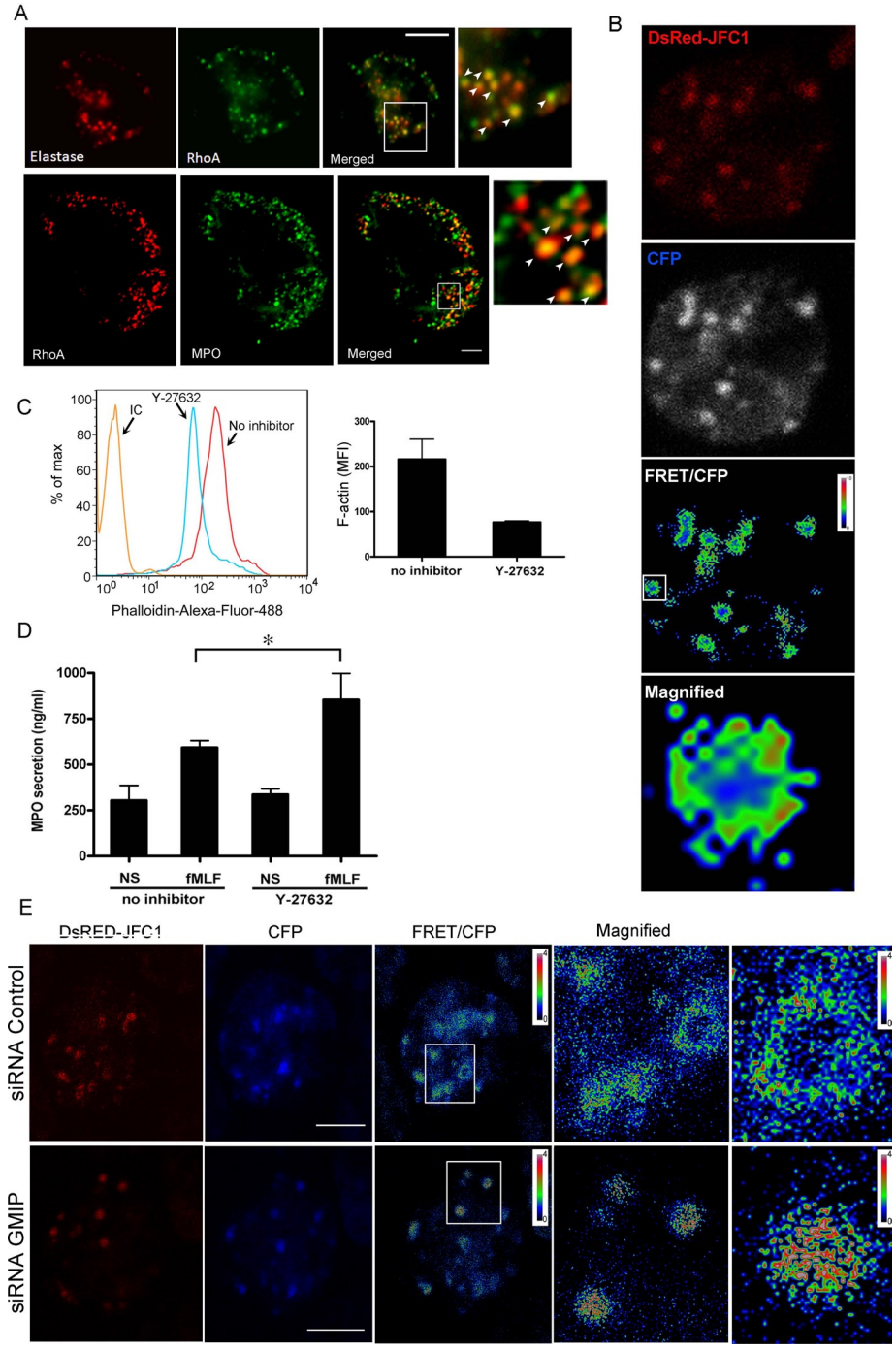

FIGURE 5: RhoA localizes at azurophilic granules and inhibition of RhoA signaling enhances exocytosis. (A) Immunofluorescence analysis of the subcellular localization of endogenous RhoA and the granule markers elastase (top panels) and myeloperoxidase (MPO, bottom panels) in human neutrophils. The insets show colocalization of RhoA with the azurophilic granule markers (white arrowheads). Scale bar: 5 μm. (B) Simultaneous analysis of RhoA activation and granule distribution in granulocytes expressing DsRED-JFC1 and a RhoA biosensor. Live-cell images were acquired by confocal microscopy, and FRET calculation was performed using Image-Pro software (Media Cybernetics, Bethesda, MD). FRET images are in pseudocolor, with the color indicating the relative value at each pixel. Active RhoA was detected polarized around some secretory granules (magnified). Representative images from three independent experiments. (C) Analysis of cortical actin polymerization in human neutrophils after treatment with the Rho-kinase inhibitor Y-27632 (5 μM). Polymerized actin was detected in fixed cells using Alexa Fluor 488–conjugated phalloidin by flow cytometry. A representative histogram is shown on the left. Experiments were performed independently using two different donors and assays were run in triplicate with similar results. Results are expressed as mean ± SD of the mean fluorescence intensity (right). (D) Mobilization of azurophilic granules is enhanced by inhibition of the RhoA-ROCK pathway. Human neutrophils (5×10^6) were incubated in the presence or absence of the ROCK-specific inhibitor and stimulated with fMLF (1 μM). Mean ± SEM from four experiments using independent donors. *, $p = 0.05$ (Mann-Whitney test). (E) Simultaneous analysis of RhoA activation and granule distribution in GMIP-deficient granulocytes expressing DsRED-JFC1. CFP, FRET, and DsRed images were obtained as described in *Materials and Methods*. Laser power and gain were maintained constant at all times and images were processed identically using Image-Pro Plus to obtain the FRET/CFP images.

(JFC1-KO) mice with the RhoA biosensor and measured RhoA activity by FRET, as described above. First, we established the experimental conditions for transfection of primary neutrophils (Figure 7A). The transfection efficiency of bone marrow–derived neutrophils by nucleofection was 25% 2 h after transfections (Figure 7A, left panel), and neutrophils were not preactivated by nucleofection (Figure 7A, middle panel). Furthermore, transfected neutrophils responded to physiological stimulation as efficiently as nontransfected cells, as determined by their elongated shape (Figure 7A, right panel). Importantly, FRET analysis of transfected cells showed significantly elevated RhoA activity in cells lacking JFC1 expression (Figure 7B).

Next we reasoned that if JFC1 modulates RhoA activity and is necessary to depolymerize actin around secretory granules to favor exocytosis, in the absence of JFC1, secretory organelles will be unable to traverse the actin barrier that separates these granules from the plasma membrane. To investigate a possible role of JFC1 in the regulation of the process of actin depolymerization associated with exocytosis of azurophilic granules, we next analyzed the subcellular localization of this set of granules in relationship to the distribution of cortical actin in wild-type and JFC1-KO neutrophils by using immunofluorescence analysis. To stimulate exocytosis, we used fMLF, an agent that induces JFC1-dependent exocytosis of a low-density, secretory subpopulation of azurophilic granules in neutrophils (Brzezinska *et al.*, 2008). In Figure 7C, we show that azurophilic granules in neutrophils lacking JFC1 are unable to traverse cortical actin upon stimulation. This is also observed in tangential images showing dorsal views of wild-type and JFC1-KO neutrophils (Figure S2). Importantly, the inability of azurophilic granules to traverse cortical

actin correlates with the deficient azurophilic granule exocytosis observed in JFC1-KO neutrophils (Figure 7D).

Finally, we reasoned that if JFC1 and GMIP operate together to control actin remodeling around secretory organelles, azurophilic granules should be trapped in cortical actin in GMIP-deficient cells as well. To test this hypothesis, we performed confocal microscopy analysis of the distribution of azurophilic granules related to cortical actin in GMIP-down-regulated HL-60 granulocytes. We found that the large majority of azurophilic granules in cells lacking GMIP are entrapped in cortical actin (Figure 8, A and B) and that granule entrapment is released by treatment with cytochalasin D (Figure 8C). Altogether, these data suggest that JFC1 and GMIP orchestrate actin remodeling around azurophilic granules to facilitate exocytosis in granulocytes.

DISCUSSION

In addition to the role played by the actin cytoskeleton as a barrier obstructing granule trafficking to the plasma membrane, cytoskeleton remodeling is proposed to actively regulate vesicular transport processes essential for regulated secretion (Muallem *et al.*, 1995; Lang *et al.*, 2000). Several discrete steps of these mechanisms remain obscure, and evidence of a direct association between the molecules of the secretory machinery with those involved in actin remodeling is currently lacking. In this work, we present evidence that the RhoA-GAP GMIP associates with the secretory factor JFC1 and regulates actin remodeling and exocytosis in granulocytes, thus establishing the first evidence of direct cross-talk between the azurophilic granule secretory machinery and the molecular components that regulate actin remodeling during regulated secretion in innate immune cells.

Our results indicate that JFC1-expressing vesicles in the exocytic active zone near the plasma membrane move in areas depleted of polymerized actin and that azurophilic granules are unable to traverse cortical actin in JFC1-KO neutrophils. Similarly, GMIP down-regulated cells show increased actin polymerization and impaired exocytosis. Finally, both JFC1-KO and GMIP-down-regulated cells have increased RhoA activity, while inhibition of the RhoA pathway decreases actin polymerization and facilitates exocytosis, further supporting a mechanism by which GMIP and JFC1, by inhibiting RhoA in the areas surrounding the secretory granules, prevent F-actin assembly to favor actin depolymerization and facilitate exocytosis.

In this study, we show that GMIP regulates vesicular trafficking. This is significant, because secretory granule movement is necessary to increase the probability of productive interactions with the plasma membrane during exocytosis (Degtyar *et al.*, 2007). The observations that azurophilic granules moving in the plane parallel to the plasma membrane undergo a significant decrease in speed in the absence of GMIP expression, which correlates with a significant decrease in granule displacement, is most likely explained by the role played by the RhoA-GAP GMIP in the prevention of actin polymerization in the areas surrounding the secretory organelles. In this way, in the absence of GMIP, increased actin polymerization would induce a semipermanent entrapment of secretory vesicles in polymerized actin. Furthermore, the observation that azurophilic granules are unable to traverse cortical actin in the absence of JFC1, suggests that JFC1 function is also necessary for the granules to remodel the actin cytoskeleton before engaging in productive interactions with the docking molecules at the plasma membrane.

In this work, we show for the first time that RhoA localizes at azurophilic granules in neutrophils. This is consistent with a possible role for RhoA in secretion and for the RhoA-GAP GMIP, in the regulation of exocytosis via inactivation of RhoA. Our data showing that RhoA activity increases at secretory organelles in GMIP-down-regulated cells, which in turn show increased actin polymerization, increased granule entrapment, and impaired exocytosis, further support this scenario. The observation that JFC1-KO cells also have increased RhoA activity further supports the idea that JFC1 and GMIP work together to mediate RhoA inactivation and induce exocytosis.

On the basis of the net increment in exocytosis observed in neutrophils in response to inhibitors of the RhoA/RhoA-kinase pathway and the decrease in exocytosis observed in GMIP-down-regulated cells, we suggest that a molecular switch from the active to the inactive form of RhoA during regulated secretion is necessary around secretory granules for neutrophils to undergo exocytosis. In this scenario, active RhoA may inhibit exocytosis by up-regulating downstream effectors, including the serine/threonine Rho kinases ROCK I and ROCK II, and LIMK (LIM kinase), with a consequent increased rate of cofilin phosphorylation (Lappalainen and Drubin, 1997; Arber *et al.*, 1998; Maekawa *et al.*, 1999), thus favoring an increase in actin polymerization in the vicinity of secretory granules, a mechanism that would be opposed by RhoA inactivation by GMIP. This is supported by our data showing that while down-regulation of GMIP increases actin polymerization and impairs exocytosis, inhibition of ROCK has the opposite effect. Alternatively, RhoA may regulate exocytosis by other mechanisms. For example, it has been proposed that RhoA regulates granule-bound phosphatidylinositol 4-kinase, leading to peripheral actin filament stabilization and exclusion of secretory granules from the exocytic active zone (Raucher *et al.*, 2000). Additionally, inhibition of vesicular fusion through RhoA-dependent kinase phosphorylation of syntaxin 1A was previously proposed (Gladycheva *et al.*, 2007). Although syntaxin 1 is not expressed in neutrophils (Brumell *et al.*, 1995), a similar effect on other syntaxins cannot be ruled out at this time. Finally, it is possible that RhoA mediates exocytosis inhibition through its antagonistic action on Rac1 (Nakayama *et al.*, 2008), a small GTPase proposed as a regulator of secretion in many cell types, including mast cells (Price *et al.*, 1995). Neutrophils express both Rac1 and 2, and a role for Rac2 in azurophilic granule secretion was demonstrated (Abdel-Latif *et al.*, 2004), but a possible antagonistic action of RhoA over Rac2 function during secretion has not been shown so far.

An important question that remains under consideration is related to the directionality of actin depolymerization that accompanies vesicular transport toward the plasma membrane. The results presented here show that polymerized actin is excluded from areas surrounding the secretory organelle and suggest that during stimulated secretion, actin depolymerization commences at the secretory organelle and subsequently depolymerizes toward the plasma membrane. Our data also suggest that secretory granules recruit a functional molecular machinery necessary to enable dismantling of the actin gel in the vicinity of the secretory organelles during exocytosis. Despite these observations, it is still unclear whether residual actin bundles may facilitate movement of the secretory vesicle in the direction of the docking site at the plasma membrane. Our results from cells treated with the actin-depolymerizing agent, cytochalasin D, show that the number of secretory organelles at the exocytic active zone increases, while vesicular movement is not abolished, and argue against a role for polymerized actin for this step of vesicular transport during exocytosis. Based on these data, the mild decrease of speed of vesicular transport observed in response to actin depolymerization induced by cytochalasin D treatment is most likely explained by a possible increment in the number of granules that are retained at docking sites at the plasma membrane. However, in a more physiological scenario, the polarized activation of RhoA in the vicinity of secretory organelles may play a regulatory role in determining the directionality of the granule movement. In this way, polarized RhoA inactivation around

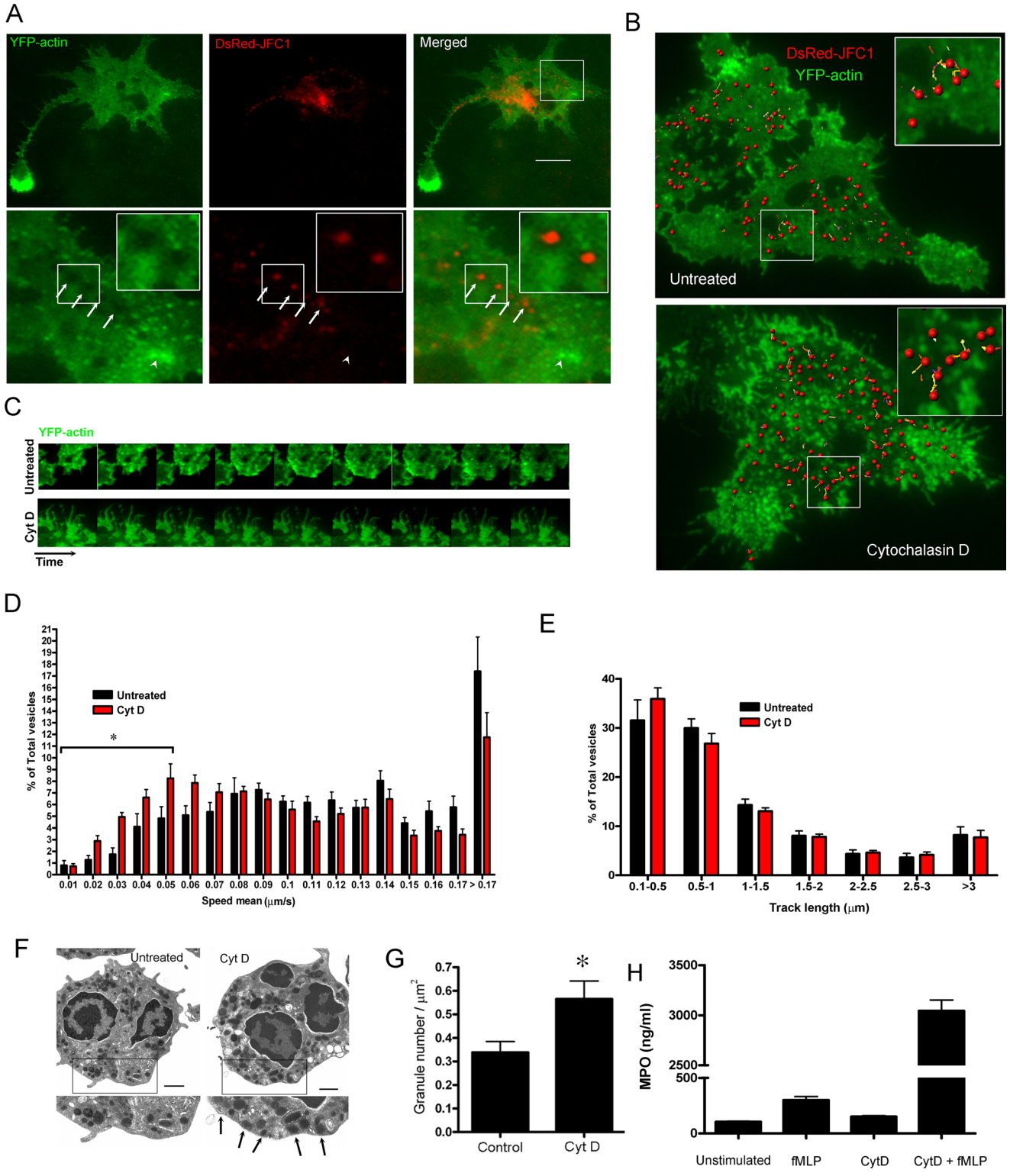

FIGURE 6: JFC1-expressing vesicles move in areas deprived of polymerized actin. (A and B) The dynamics of JFC1-expressing vesicles was analyzed by TIRFM in HL-60 cells expressing the vesicular marker DsRED-JFC1 and YFP-actin. (A) Granules containing JFC1 exclude polymerized actin from surrounding areas (arrows, bottom panel magnification) and do not visit areas with high actin turnover (arrowhead, bottom panel magnification). A halo deprived of polymerized actin is frequently observed surrounding JFC1-expressing granules (further magnification is shown in inset). Scale bar: 5 μm. (B) Vesicular dynamics of JFC1-expressing granules. Images were acquired at 1-s intervals for 2 min. Exposure time was 300 ms. Images were analyzed using Imaris (version 7.0) software (Bitplane Scientific Software). Scale bar: 10 μm. The insets show a magnification of the vesicular dynamics for untreated or cytochalasin D-treated (10 μg/ml) cells. Each sphere represents a vesicle. The tracks indicate the trajectory of the associated vesicles occurring during the analysis. Actin remodeling and vesicular dynamics in untreated or cytochalasin D-treated cells are shown in Movies S3 and S4,

secretory organelles may facilitate granule movement toward areas deprived of polymerized actin, while active RhoA-initiated discrete actin polymerization may provide the driving force to induce movement toward areas free of polymerized actin.

From the data presented here, it is evident that JFC1 and GMIP participate in the organization of the actin cytoskeleton around secretory granules to favor exocytosis, but the regulation of this mechanism upon stimulation of secretion requires further investigation. A possible mechanism of activation may be mediated by posttranslational modification of JFC1 (i.e., phosphorylation) in response to stimulation with chemotactic peptides, which in turn would facilitate recruitment of and interaction with GMIP at the surface of secretory organelles. Alternatively, JFC1 conformational changes by phosphorylation may not affect binding to GMIP but may instead facilitate RhoA-GAP activation and a concomitant decrease of active RhoA at the granule-surrounding areas. A possible role for JFC1 regulation by phosphorylation during exocytosis in granulocytes is supported by previous studies showing that fMLF-mediated neutrophil stimulation induces Akt activation (Burelout *et al.*, 2007), and that JFC1 is an Akt substrate in vivo (Johnson *et al.*, 2005b). Also, JFC1-dependent activation of the RhoA-GAP of GMIP may induce not only inactivation but also redistribution of RhoA toward cellular compartments other than secretory organelles in which RhoA may again become active. In this scenario, granule-associated RhoA activity would decrease in response to fMLF stimulation, but total RhoA activity in the cell might not change or might even increase. Thus the activity of granule-associated RhoA, rather than total RhoA activity, would be important for vesicular transport and exocytosis. Another possibility is that, in response to fMLF stimulation, GMIP is recruited to azurophilic granules by molecules other than JFC1. A possible candidate to perform this function is Gem, a small GTPase of the RGK (Rad, Gem, Kir) family, which interacts with GMIP (Aresta *et al.*, 2002) and is known to regulate exocytosis (Sasaki *et al.*, 2005). In this hypothetical model, Rab27a-bound JFC1 would favor GMIP RhoA-GAP activity on secretory organelles upon stimulation to mediate RhoA inactivation and thus increase granule transport toward the plasma membrane.

In conclusion, our work suggests that secretory granules contain the necessary molecular machinery to prevent actin polymerization in their surrounding areas to facilitate vesicle movement toward the exocytic active zone. Furthermore, we have identified JFC1 and GMIP as key regulators of this mechanism in neutrophils, which suggests they are important players in innate immunity and inflammation.

MATERIAL AND METHODS

Materials

LPS (*Escherichia coli*, serotype R515) was obtained from Alexis Biochemicals (San Diego, CA). The chemotactic peptide fMLF was obtained from Sigma-Aldrich (St. Louis, MO). Paraformaldehyde was from Electron Microscopy Sciences (Hatfield, PA).

Experimental animal model

The JFC1/Sytl1-knockout mouse (Sytl1$^{tm1a(KOMP)Wtsi}$) was generated by the Knockout Mouse Project (KOMP) repository and made available to us through the Wellcome Trust Sanger Institute. The KOMP repository is the official archive and distribution center for KOMP, a major 5-yr trans–National Institutes of Health (NIH) initiative designed to generate new null alleles in C57BL/6 embryonic stem cells for the generation of knockout mice. The *sytl1* gene was targeted by using a trapping cassette (conditional targeted trap) "SA-βgeo-pA" (splice acceptor-beta-geo-polyA) flanked by Flp-recombinase target sites to create a constitutively null mutation in the *sytl1* gene in chromosome 4 through efficient splicing to the reporter cassette, resulting in the truncation of the endogenous transcript. The Sytl1$^{tm1a(KOMP)Wtsi}$ was genotyped using tail-extracted genomic DNA and genotyping reactions consisting of a combination of separate PCRs to detect LacZ, the gene-specific wild-type allele, and a mutant allele-specific short-range PCR. The following primers were used (5′→3′, primer name, sequence): CAS-Rl-Term, TCGTGGTATCGTTATGCGCC; Sytl1-44240 F, TAAATGCCAGGGGAAAGGTG; Sytl1-44240 R, TGGGATTCTCCAGGTTGAGC; LacZ-2-small-F, ATCACGACGCGCTGTATC; and LacZ-2-small-R, ACATCGGGCAAATAATATCG. Primers were used to amplify a 316–base pair mutant (Sytl1F-CAS-Rl-Term), 334–base pair wild-type (Sytl1F- Sytl1R), and 108–base pair LacZ PCR products (LacZF-LacZR). All animal studies were performed in compliance with the U.S. Department of Health and Human Services and the NIH and were approved by the Institutional Review Board at the Scripps Research Institute.

Neutrophil isolation

Human neutrophils were isolated from normal donor's blood by Ficoll density centrifugation as previously described (Markert *et al.*, 1984). For sucrose-density-gradient fractionation, neutrophils were treated with diisopropylfluorophosphate to inhibit intrinsic proteases and lysed by nitrogen cavitation, which preserves the structures of intracellular organelles. To this end, lysates were spun down at 400 × *g* for 30 min, and the supernatants were placed on top of a continuous sucrose gradient (10–70%) and spun down at 150,000 × *g* for 1 h at 4°C. Aliquots were collected from the top to the bottom and analyzed for the expression of granule markers (Munafo *et al.*, 2007). Bone marrow–derived neutrophils (BM-PMNs) were isolated using a Percoll-gradient fractionation system as described previously (Johnson *et al.*, 2010b).

Transfection of bone marrow–derived neutrophils

Bone marrow–derived neutrophils (BM-PMNs) were transfected by nucleofection using the Amaxa P3 Primary Cell 4D-Nucleofector

respectively. (C) Time-lapse image showing actin remodeling in untreated or cytochalasin D-treated (Cyt D) cells. The interval between the images shown is 5 s. (D and E) Quantitative analysis of vesicular dynamics was performed using 10 untreated and 12 cytochalasin D-treated cells from two independent experiments. A total of 2743 (untreated) and 2692 (Cyt D) vesicles were analyzed in these studies. (D) Histograms of the speed of JFC1-expressing granules from untreated or cytochalasin D-treated cells. Granule speeds were binned in 0.01-μm/s increments and plotted as a percentage of total granules for a given cell. Results are represented as mean ± SEM.*, $p < 0.05$. (E) Measurements of vesicular track length are shown in histograms. (F) Transmission electron microscopy analysis of resting human neutrophils (Untreated) and neutrophils treated with cytochalasin D (Cyt D). The arrows indicate vesicles detected in close proximity to the plasma membrane. (G) The number of granules at the exocytic active zone significantly increases in response to inhibition of actin remodeling. Cells were treated with cytochalasin D or left untreated and the number of granules at the exocytic active zone was quantified using TIRFM (*, $p < 0.05$). (H) Inhibition of actin remodeling facilitates exocytosis in neutrophils. Human neutrophils were treated with cytochalasin D and subsequently stimulated with fMLF for 10 min. Secreted MPO was analyzed by ELISA. Triplicate of one representative experiment is shown.

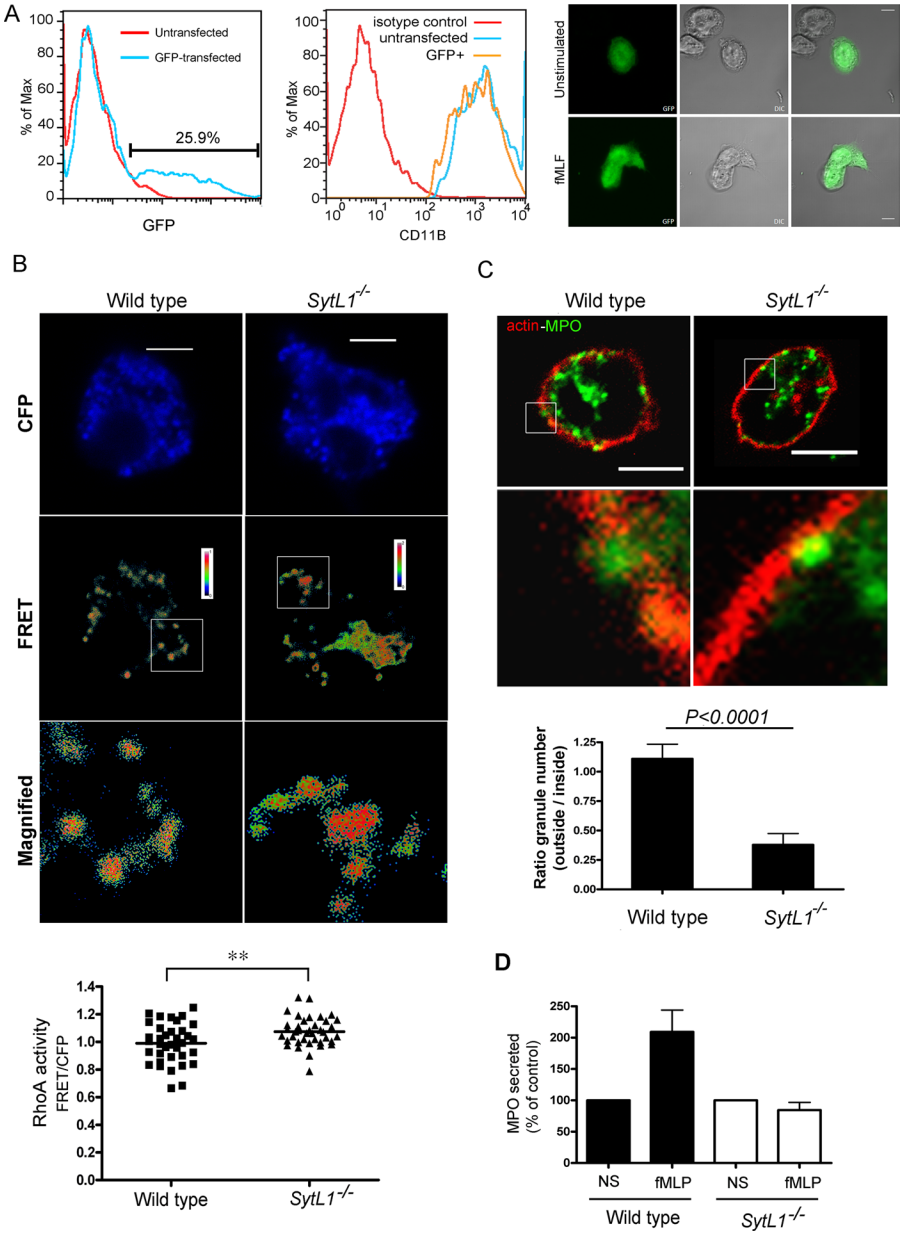

FIGURE 7: Azurophilic granules are unable to traverse cortical actin in neutrophils lacking JFC1. (A) Transfection of primary neutrophils by nucleofection. BM-PMNs were isolated and transfected using a GFP expression vector (top, left panel). Transfected cells are not pre-activated (top, middle panel) and are responsive to stimulation (top, right panel). (B) Analysis of RhoA distribution and activation in primary neutrophils from JFC1 knockout mice (*SytL1*$^{-/-}$) or wild-type control mice transfected with a RhoA biosensor. FRET analysis and calculation was performed as described in *Materials and Methods* and in Figure 5. FRET images are in pseudocolor, with the color indicating the relative value at each pixel. RhoA activity (FRET/CFP) was significantly higher in neutrophils lacking JFC1 ($p < 0.01$; n = 36 [Wild type] and 39 [*SytL1*$^{-/-}$]) from two independent experiments (Mann-Whitney test). (C) Azurophilic granules are unable to traverse cortical actin in the absence of JFC1. Untransfected BM-PMNs from the JFC1 knockout mice (*SytL1*$^{-/-}$) or wild-type control mice were stimulated with fMLF for 10 min, fixed, and analyzed by confocal microscopy after staining for endogenous MPO (green) or actin (rhodamine-phalloidin; red). The ratio between the number of granules that traversed cortical actin (outside) and those adjacent to the inner side of cortical actin (inside) were quantified in *z*-sections covering the entire cell and expressed as the ratio of the number of granules located outside/inside for each cell. The results are expressed as mean ± SEM from a total of 22 wild-type and 22 JFC1-KO cells from three independent experiments (Mann-Whitney test). (D) Wild-type or JFC1-KO (*SytL1*$^{-/-}$) neutrophils were stimulated with fMLF and secreted MPO was analyzed by ELISA. Mean ± SEM (n = 3).

X kit L and a 4D-Nucleofector System (Lonza AG, Allendale, NJ). Briefly, 2.5×10^6 cells were resuspended in 100 µl of nucleofection solution P3, transferred to a nucleofection cuvette, and after addition of 2–5 µg of the indicated expression vector, the cells were immediately pulsed using the human monocytes setup in the 4D-Nucleofector System. After addition of 300 µl of Roswell Park Memorial Institute (RPMI) medium (no serum), the cells were transferred to an 8-well Lab-Tek chambered #1.0 borosilicate coverglass system or to 1.5-ml polypropylene tubes containing RPMI medium. The cells were recovered and used in fluorescence or functional assays 2 h after transfection. Transfection efficiency was ~20%, and transfected cells were not preactivated by the nucleofection procedure and were perfectly functional (Figure 7A).

Stimulated secretion in SLO-permeabilized neutrophils

Secretory assays using SLO-permeabilized neutrophils were performed as previously described (Brzezinska *et al.*, 2008). Briefly, human neutrophils ($2.5–5 \times 10^6$) or BM-derived mouse neutrophils (1×10^6) were washed twice with phosphate-buffered saline (PBS), resuspended in permeabilization buffer (100 µl; Imai *et al.*, 2004), and transferred to a tube containing SLO (2 µl of 2500 U/ml) in the presence of the indicated antibodies (50 µg/ml) and incubated at 37°C for 5 min. Where indicated, the cells were incubated with lipopolysaccharide (LPS; 100 ng/ml, preincubated with autologous serum) for 60 min and stimulated with fMLF (1 µm) for an additional 10 min. The reactions were stopped by transferring the samples to ice; samples were then immediately spun at 16,000 × *g* at 4°C for 5 min. Supernatants were stored at –20°C until the assays were performed. For MPO secretion assays in nonpermeabilized neutrophils, the reactions were carried on in RPMI without serum. The analysis of secreted and total cell lysate myeloperoxidase was performed using a human- or murine-specific MPO enzyme-linked immunosorbent assay (ELISA; Assay Designs [Farmingdale, NY] and HyCult Biotech [Plymouth Meeting, PA], respectively) according to the manufacturers' instructions. Importantly, MPO detection using these methods is highly sensitive (50 pg of MPO) and allows for the detection of MPO secreted from human or murine neutrophils in the absence of cytoskeleton-disrupting agents.

Mobilization of CD11b in murine neutrophils

Transfected or untransfected BM-derived neutrophils were immunostained for 1 h at

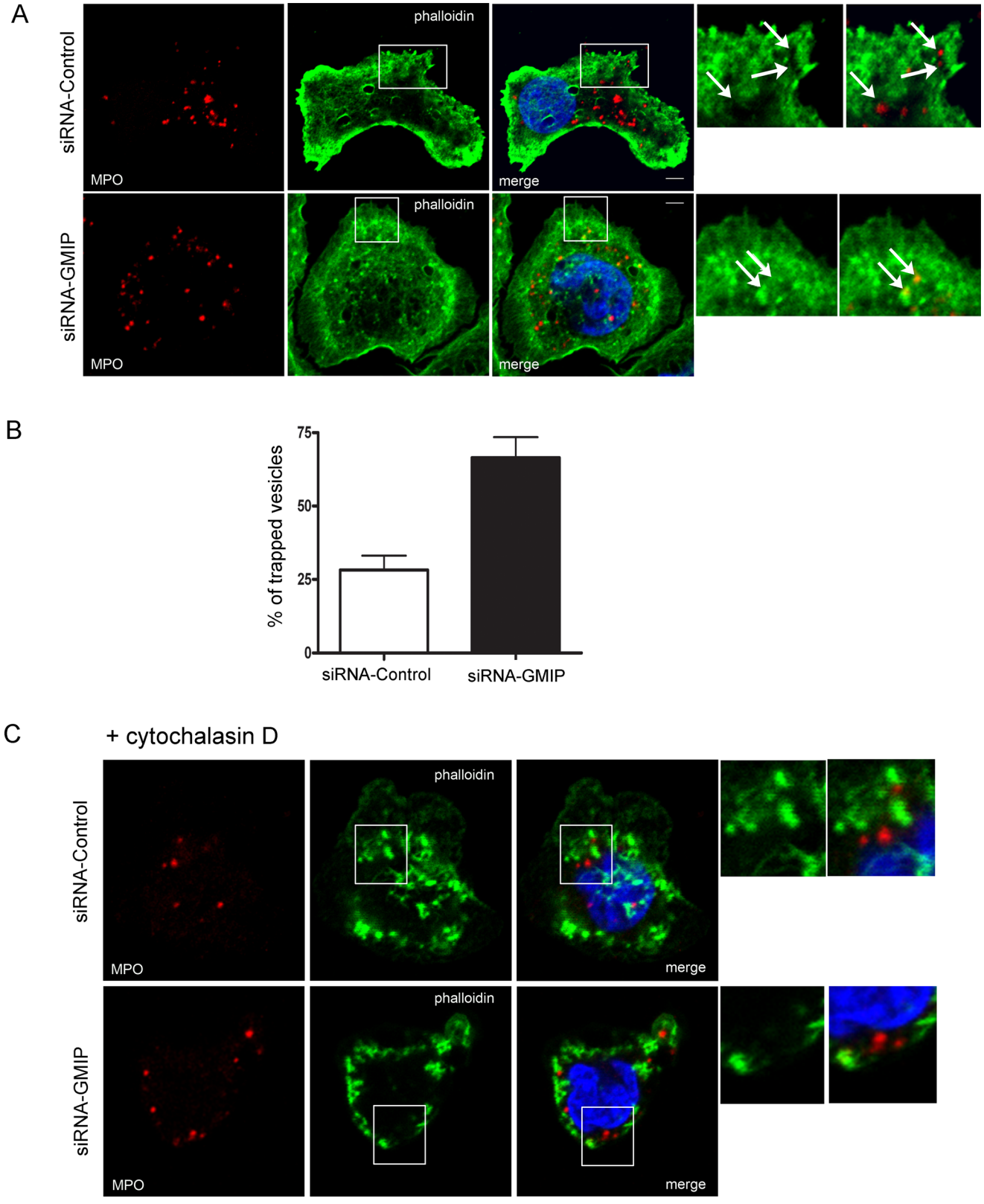

FIGURE 8: GMIP-deficient cells have increased number of azurophilic granules trapped in cortical actin, which are released upon cytoskeleton depolymerization. (A) GMIP-deficient and control HL-60 granulocytes were stimulated with fMLF for 10 min, fixed, and analyzed by confocal microscopy after staining for endogenous MPO (green) or actin (rhodamine-phalloidin; red). B) The number of granules showing a halo of depolymerized actin and those trapped in cortical actin were quantified, and results are expressed as mean ± SEM. (C) The cells were treated with cytochalasin D before fixation to induce actin depolymerization and granules were visualized by immunofluorescence confocal microscopy as described in *Materials and Methods*.

4°C with monoclonal anti-CD11b-phycoerythrin (anti-CD11b-PE). PE-conjugate mouse immunoglobulin G (IgG) 2b was used as isotype control. Neutrophils were washed and subsequently fixed in 1% paraformaldehyde. Neutrophils were gated based on GFP expression, and the specific CD11b staining was determined. Data were collected using a FACSCalibur flow cytometer (BD Biosciences, Franklin Lakes, NJ) and analyzed using FlowJo software (Ashland, OR).

Differentiation and transfection of HL-60 promyelocytic cells

The human promyelocytic leukemia cell line HL-60 (American Type Culture Collection, Manassas, VA) was cultured in Iscove's Modified Dulbecco's Medium (Invitrogen, Carlsbad, CA) supplemented with 20% fetal bovine serum (Hyclone, Logan, UT), 0.292 mg/ml glutamine, 50 U/ml penicillin, and 50 μg/ml streptomycin at 37°C in 5% CO_2/air. For differentiation, HL-60 cells were treated with dimethyl sulfoxide (DMSO; 1.3%, vol/vol) or PMA (phorbol, 12-myristate, 13-acetate; 3.2 nM) or left untreated for 48 h at 37°C in 5% CO_2/air. HL-60 cells (5×10^6) were transfected by nucleofection with ON-TARGET GMIP-specific siRNA oligonucleotides (single siRNA Cat# j021160-10; Dharmacon, Lafayette, CO) or control nonsilencing siRNA (Dharmacon) using solution V and electrical setting T01. For expression vectors, the cells were subsequently transfected by nucleofection using the electrical setting X01 as described previously (Brzezinska *et al.*, 2008). The cells were differentiated and used 48–72 h after transfection. In some experiments, the cells were harvested, lysed as previously described (Munafo *et al.*, 2007), and analyzed by Western blotting for the expression of GMIP. In some experiments, GMIP expression was also detected by immunofluorescence and confocal microscopy analysis.

TIRFM and data analysis

For live-cell TIRFM imaging, HL-60 cells were seeded in 8-well plates with bottom coverglass (1.5 Lab-Tek borosilicate coverglass; Nunc, Thermo) in phenol red–free RPMI medium. The cells were transferred to a prewarmed microscope stage. TIRFM experiments were performed using a 100 × 1.45 numerical aperture (NA) TIRF objective (Nikon, Melville, NY) on a Nikon TE2000U microscope custom-modified with a TIRF illumination module. Laser illumination (488 and 543 laser lines) was adjusted to impinge on the coverslip at an angle to yield a calculated evanescent field depth (d) < 100 nm. Images were acquired on a 14-bit, cooled charge-coupled device camera (Hamamatsu) controlled through NIS-Elements software (Nikon). The images were recorded at 1-s intervals using exposure times of 200–600 ms, depending on the intensity of the signal. Images were analyzed using ImageJ (version 1.43) and Imaris (version 7.0) software (Bitplane Scientific Software, South Windsor, CT). All data analysis was performed by tracking granule movement through all frames of the movies. All vesicles that appeared in the TIRFM zone for at least three consecutive frames during the length of the study were included in the analysis. Images that experienced mild fading over time were auto-thresholded in Imaris to ensure that regions of interest (vesicle center or centroid) were continually tracked throughout the period monitored.

Mass spectrometry analysis

JFC1-coimmunoprecipitating proteins were detected using microcapillary reverse-phase high-performance liquid chromatography (HPLC)–nanoelectrospray tandem mass spectrometry (MS/MS). For this purpose, endogenous JFC1 was immunoprecipitated from human neutrophils, samples were resolved by gel electrophoresis in 10% Bis-Tris NuPAGE gels, and proteins were visualized with Simply Blue Coomassie Blue staining (Invitrogen). A band identified in the samples as immunoprecipitating with the anti-JFC1 specific antibody was excised and then divided in half for separate in-gel AspN and chymotryptic digestions after reduction and carboxyamido-methylation. The resultant digests were pooled just before HPLC–MS/MS injection. The sequence analysis was performed at the Harvard Microchemistry Facility using a 75-μm reverse-phase microcolumn terminating in a custom nanoelectrospray source directly coupled to a LCQ DECA XP Plus quadrupole ion-trap mass spectrometer (Thermo-Finnigan, West Palm Beach, FL) as previously described (Pacquelet *et al.*, 2007). MS/MS spectra were acquired with relative collision energy of 30% and an isolation width of 2.5 Da. Recurring ions were dynamically excluded. After database correlation with the algorithm SEQUEST (Eng *et al.*, 1994), identified peptides were confirmed by manual de novo interpretation of the MS/MS spectra using FuzzyIons (Chittum *et al.*, 1998).

Immunofluorescence, FRET, and confocal microscopy analysis

Neutrophils or HL-60 cells were seeded at 70% confluence in an eight-well chambered coverglass, fixed with 3.7% paraformaldehyde, permeabilized, and blocked with a solution of PBS containing 0.01% saponin and 1% BSA. To stain the nucleus, some samples were incubated with 4′,6-diamidino-2-phenylindole, dihydrochloride (DAPI) for 5 min at 21°C. Samples were labeled with the indicated primary antibodies overnight at 4°C and then with the appropriate combination of the secondary antibodies Alexa-Fluor–conjugated (488 and/or 594) donkey anti-rabbit, anti-mouse, and/or anti-goat (Molecular Probes, Invitrogen). Controls in the absence of primary antibodies were always run in parallel. Cells were stored in Fluoromount-G (Southern Biotechnology, Birmingham, AL) and analyzed using a Zeiss LSM 710 laser-scanning confocal microscope attached to a Zeiss Observer Z1 microscope using the 100× or 63× oil Plan Apo, 1.4 NA infinity-corrected optics. For visualization, fluorescence associated with Alexa Fluor 594–labeled secondary antibody was excited using the 543-nm laser line and was collected using a standard Texas Red filter. Fluorescence associated with Alexa Fluor 488–labeled secondary antibodies was visualized using the 488-nm laser line and collected using a standard fluorescein isothiocyanate (FITC) filter set. Images were analyzed using ImageJ and processed with Adobe Photoshop CS4 (San Jose, CA). Where indicated, for the analysis of the distribution of endogenous MPO and GMIP, we used TIRFM microscopy analysis of fixed cells. To this end, neutrophils were transferred to chambered coverglass (Lab-Tek 1.5, Nunc), fixed and permeabilized, and blocked as described at the beginning of this paragraph. Samples were labeled with anti-MPO-specific antibody (HyCult Biotech), anti-GMIP antibodies (described in the *Antibodies* section) or control antibodies overnight at 4°C and with species-specific Alexa-conjugated secondary antibodies (Invitrogen). The cells were stored in unsolidified water-based mounting medium (refractive index = 1.37) until analyzed. TIRFM experiments were performed as described in the *TIRFM* section, except that the images were recorded using 300- to 500-ms exposure times, depending on the intensity of the signal. Images were analyzed using ImageJ software.

For live-cell FRET analysis of RhoA activity, HL-60 cells were transfected by nucleofection with the expression vector pTriEx-RhoA biosensor wild type. In some experiments, cells were cotransfected with the RhoA biosensor and the expression vector pDsred-JFC1. The RhoA biosensor, designed by Klaus Hahn and collaborators (Pertz *et al.*, 2006), consists of a small RhoA-binding domain (RBD)

derived from the RhoA effector Rhotekin, enhanced cyan fluorescent protein (ECFP), an unstructured linker of optimized length, pH-insensitive Citrine-YFP, and a full-length RhoA. In this probe, the C-terminus of the RhoA is free of any modifications so as to maintain the integrity of regulation of RhoA by GDI (guanine nucleotide dissociation inhibitor; Pertz *et al.*, 2006). To avoid potential toxicity from GTPase overexpression, low expressers were selected. CFP, FRET, YFP, and DsRed images were captured using a Zeiss LSM 710 laser-scanning confocal microscope attached to a Zeiss Observer Z1 microscope using the 63× oil Plan Apo, 1.4 NA infinity-corrected optics. To avoid uneven photobleaching of donor and acceptor, high-resolution, single, 1-micron optical slices of the cell were taken and time lapses were avoided. For FRET/CFP ratiometric image processing, we followed the procedure described by Pertz and collaborators (Pertz *et al.*, 2006), using ImagePro Plus Software (Media Cybernetics, Bethesda, MD). The final FRET images were displayed in pseudocolor scaled linearly from the lowest to the highest signal within each cell using ImageJ.

Gel electrophoresis and Western blotting

Proteins were separated by gel electrophoresis using NuPAGE gels and MOPS buffer (Invitrogen). Proteins were transferred onto nitrocellulose membranes and the membranes were blocked with PBS containing 5% (wt/vol) blotting-grade nonfat dry milk blocker (Bio-Rad, Hercules, CA). The proteins were detected by probing the membranes with the indicated primary antibodies at appropriate dilutions. The detection system used horseradish peroxidase–conjugated secondary antibodies (Bio-Rad) and the SuperSignal West Pico chemiluminescence substrate system (Thermo, West Palm Beach, FL). Transferred proteins were visualized using Hyperfilm (Amersham Bioscience, Piscataway, NJ).

Antibodies

The antibodies phycoerythrin (PE)-conjugated anti–mouse CD11b and PerCP- or FITC-conjugated anti–mouse Ly-6G (clone A18) were obtained from BD PharMingen (San Diego, CA). We also used anti–mouse MPO (HyCult Biotech) as well as anti–human MPO (BioDesign). Anti-neutrophil elastase was from Calbiochem (San Diego, CA). The polyclonal antibody against an amino-terminal peptide from human JFC1 was described previously (McAdara-Berkowitz *et al.*, 2001). The anti-GMIP polyclonal antibody was raised in rabbits against the peptide EGRKRYSDIFRSLD. This antibody recognizes both murine and human GMIP. We also used rabbit anti-GMIP and mouse anti-RhoA from Santa Cruz Biotechnology (Santa Cruz, CA).

Vectors and cloning

The various steps in the cloning of the constructs were performed by standard techniques and all constructs were verified by sequencing. The various *jfc1* DNA fragments cloned into the *Eco*RI/*Sal*I sites of the pGEX-6P1 polylinker were generated by PCR using *jfc1* cDNA and primers described before (Catz *et al.*, 2002). The DsRED-JFC1 and the EGFP-LAMP-3 vectors were described previously (Johnson *et al.*, 2005a; Brzezinska *et al.*, 2008); the pTriEx-RhoA biosensor was described previously (Pertz *et al.*, 2006) and acquired through Addgene. The vector for the expression of YFP-actin was obtained from Clontech (Mountain View, CA).

GMIP pulldown assays

For pulldown assays, 85 pmol of the indicated GST-fusion proteins were bound to 30 µl of prewashed glutathione-Sepharose 4B (Amersham Biosciences). Beads were washed with PBS and utilized to pull down GMIP by incubation with neutrophil lysates (9×10^7 cell equivalents). Recombinant proteins and lysates were rotated overnight at 4°C in binding buffer consisting of 0.5% Triton-X100, 136 mM NaCl, PBS (pH 7.4), containing anti-proteases (EDTA-free Complete; Roche, Indianapolis, IN). Beads were washed three times with wash buffer (PBS containing 0.05% Tween-20) and once with ice-cold PBS. The proteins in the pulldown were resuspended in sample buffer, samples were resolved by NuPAGE gel electrophoresis, and GMIP was detected by Western blotting.

GTP-RhoA pulldown assay

The RhoA pulldown assay was performed using 50 µg RBD of the GTPase effector Rhotekin as a GST fusion protein (GST-Rhotekin-RBD) bound to beads to pull down GTP-bound RhoA from GMIP-down-regulated or control 293T cells exactly as previously described (Pellegrin and Mellor, 2008).

Statistical analysis

Data are presented as means, and error bars correspond to SEM. Statistical significance was determined using the unpaired Student's *t* test or the Mann-Whitney test using GraphPad InStat 3, and graphs were made using GraphPad Prism 4. Differences were considered statistically significant at $p < 0.05$.

ACKNOWLEDGMENTS

The work was supported by U.S. Public Health Service Grant HL088256 to S.D.C. This work was supported in part by a postdoctoral fellowship from the American Heart Association to J.M. We thank Malcolm Wood for help with electron microscopy and Tho Ta for his help with animal work. We also thank Celine DerMardirossian for her contribution of GST-Rhotekin-RBD and advice on RhoA pulldown assays.

REFERENCES

Abdel-Latif D, Steward M, Macdonald DL, Francis GA, Dinauer MC, Lacy P (2004). Rac2 is critical for neutrophil primary granule exocytosis. Blood 104, 832–839.

Arber S, Barbayannis FA, Hanser H, Schneider C, Stanyon CA, Bernard O, Caroni P (1998). Regulation of actin dynamics through phosphorylation of cofilin by LIM-kinase. Nature 393, 805–809.

Aresta S, de Tand-Heim MF, Beranger F, de Gunzberg J (2002). A novel Rho GTPase-activating-protein interacts with Gem, a member of the Ras superfamily of GTPases. Biochem J 367, 57–65.

Bretschneider T, Diez S, Anderson K, Heuser J, Clarke M, Muller-Taubenberger A, Kohler J, Gerisch G (2004). Dynamic actin patterns and Arp2/3 assembly at the substrate-attached surface of motile cells. Curr Biol 14, 1–10.

Brovkovych V, Gao XP, Ong E, Brovkovych S, Brennan ML, Su X, Hazen SL, Malik AB, Skidgel RA (2008). Augmented inducible nitric oxide synthase expression and increased NO production reduce sepsis-induced lung injury and mortality in myeloperoxidase-null mice. Am J Physiol Lung Cell Mol Physiol 295, L96–L103.

Brown GE, Stewart MQ, Liu H, Ha VL, Yaffe MB (2003). A novel assay system implicates PtdIns(3,4)P_2, PtdIns(3)P, and PKCδ delta in intracellular production of reactive oxygen species by the NADPH oxidase. Mol Cell 11, 35–47.

Brumell JH, Volchuk A, Sengelov H, Borregaard N, Cieutat AM, Bainton DF, Grinstein S, Klip A (1995). Subcellular distribution of docking/fusion proteins in neutrophils, secretory cells with multiple exocytic compartments. J Immunol 155, 5750–5759.

Brzezinska AA, Johnson JL, Munafo DB, Crozat K, Beutler B, Kiosses WB, Ellis BA, Catz SD (2008). The Rab27a effectors JFC1/Slp1 and Munc13–4 regulate exocytosis of neutrophil granules. Traffic 9, 2151–2164.

Burelout C, Naccache PH, Bourgoin SG (2007). Dissociation between the translocation and the activation of Akt in fMLP-stimulated human neutrophils–effect of prostaglandin E2. J Leukoc Biol 81, 1523–1534.

Catz SD (2008). Characterization of Rab27a and JFC1 as constituents of the secretory machinery of prostate-specific antigen in prostate carcinoma cells. Methods Enzymol 438, 25–40.

Catz SD, Johnson JL, Babior BM (2002). The C2A domain of JFC1 binds to 3′-phosphorylated phosphoinositides and directs plasma membrane association in living cells. Proc Natl Acad Sci USA 99, 11652–11657.

Chittum HS, Lane WS, Carlson BA, Roller PP, Lung FD, Lee BJ, Hatfield DL (1998). Rabbit β-globin is extended beyond its UGA stop codon by multiple suppressions and translational reading gaps. Biochemistry 37, 10866–10870.

Clark SR *et al.* (2007). Platelet TLR4 activates neutrophil extracellular traps to ensnare bacteria in septic blood. Nat Med 13, 463–469.

Cockcroft S (1991). Relationship between arachidonate release and exocytosis in permeabilized human neutrophils stimulated with formylmethionyl-leucyl-phenylalanine (fMetLeuPhe), guanosine 5′-[gamma-thio] triphosphate (GTP[S]) and Ca2+. Biochem J 275, 127–131.

Degtyar VE, Allersma MW, Axelrod D, Holz RW (2007). Increased motion and travel, rather than stable docking, characterize the last moments before secretory granule fusion. Proc Natl Acad Sci USA 104, 15929–15934.

Ehrlich JS, Hansen MD, Nelson WJ (2002). Spatio-temporal regulation of Rac1 localization and lamellipodia dynamics during epithelial cell-cell adhesion. Dev Cell 3, 259–270.

Eng JK, McCormack AL, Yates JR, III (1994). An approach to correlate tandem mass spectral data of peptides with amino acid sequences in a protein database. J Am Soc Mass Spectrom 5, 976–989.

Feldmann J *et al.* (2003). Munc13–4 is essential for cytolytic granules fusion and is mutated in a form of familial hemophagocytic lymphohistiocytosis (FHL3). Cell 115, 461–473.

Fukuda M (2002). Synaptotagmin-like protein (Slp) homology domain 1 of Slac2-a/melanophilin is a critical determinant of GTP-dependent specific binding to Rab27A. J Biol Chem 277, 40118–40124.

Gladycheva SE, Lam AD, Liu J, D'Andrea-Merrins M, Yizhar O, Lentz SI, Ashery U, Ernst SA, Stuenkel EL (2007). Receptor-mediated regulation of tomosyn-syntaxin 1A interactions in bovine adrenal chromaffin cells. J Biol Chem 282, 22887–22899.

Hatzoglou A, Ader I, Splingard A, Flanders J, Saade E, Leroy I, Traver S, Aresta S, de Gunzberg J (2007). Gem associates with Ezrin and acts via the Rho-GAP protein Gmip to down-regulate the Rho pathway. Mol Biol Cell 18, 1242–1252.

Hendrix A, Braems G, Bracke M, Seabra M, Gahl W, De Wever O, Westbroek W (2010). The secretory small GTPase Rab27B as a marker for breast cancer progression. Oncotarget 1, 304–308.

Holt O, Kanno E, Bossi G, Booth S, Daniele T, Santoro A, Arico M, Saegusa C, Fukuda M, Griffiths GM (2008). Slp1 and Slp2-a localize to the plasma membrane of CTL and contribute to secretion from the immunological synapse. Traffic 9, 446–457.

Hoppe AD, Swanson JA (2004). Cdc42, Rac1, and Rac2 display distinct patterns of activation during phagocytosis. Mol Biol Cell 15, 3509–3519.

Imai A, Yoshie S, Nashida T, Shimomura H, Fukuda M (2004). The small GTPase Rab27B regulates amylase release from rat parotid acinar cells. J Cell Sci 117, 1945–1953.

Jog NR, Rane MJ, Lominadze G, Luerman GC, Ward RA, McLeish KR (2007). The actin cytoskeleton regulates exocytosis of all neutrophil granule subsets. Am J Physiol Cell Physiol 292, C1690–C1700.

Johnson JL, Brzezinska AA, Tolmachova T, Munafo DB, Ellis BA, Seabra MC, Hong H, Catz SD (2010a). Rab27a and Rab27b regulate neutrophil azurophilic granule exocytosis and NADPH oxidase activity by independent mechanisms. Traffic 11, 533–547.

Johnson JL, Ellis BA, Noack D, Seabra MC, Catz SD (2005a). The Rab27a binding protein JFC1 regulates androgen-dependent secretion of prostate specific antigen and prostate specific acid phosphatase. Biochem J 391, 699–710.

Johnson JL, Hong H, Monfregola J, Kiosses WB, Catz SD (2010b). MUNC13–4 restricts motility of RAB27A-expressing vesicles to facilitate lipopolysaccharide-induced priming of exocytosis in neutrophils. J Biol Chem 286, 5647–5656.

Johnson JL, Pacquelet S, Lane WS, Eam B, Catz SD (2005b). Akt regulates the subcellular localization of the Rab27a-binding protein JFC1 by phosphorylation. Traffic 6, 667–681.

Kuhn JR, Pollard TD (2005). Real-time measurements of actin filament polymerization by total internal reflection fluorescence microscopy. Biophys J 88, 1387–1402.

Lang T, Wacker I, Wunderlich I, Rohrbach A, Giese G, Soldati T, Almers W (2000). Role of actin cortex in the subplasmalemmal transport of secretory granules in PC-12 cells. Biophys J 78, 2863–2877.

Lappalainen P, Drubin DG (1997). Cofilin promotes rapid actin filament turnover in vivo. Nature 388, 78–82.

Maekawa M, Ishizaki T, Boku S, Watanabe N, Fujita A, Iwamatsu A, Obinata T, Ohashi K, Mizuno K, Narumiya S (1999). Signaling from Rho to the actin cytoskeleton through protein kinases ROCK and LIM-kinase. Science 285, 895–898.

Manneville JB, Etienne-Manneville S, Skehel P, Carter T, Ogden D, Ferenczi M (2003). Interaction of the actin cytoskeleton with microtubules regulates secretory organelle movement near the plasma membrane in human endothelial cells. J Cell Sci 116, 3927–3938.

Markert M, Andrews PC, Babior BM (1984). Measurement of O_2^- production by human neutrophils. The preparation and assay of NADPH oxidase-containing particles from human neutrophils. Methods Enzymol 358–365.

McAdara-Berkowitz JK, Catz SD, Johnson JL, Ruedi JM, Thon V, Babior BM (2001). JFC1, a novel tandem C2 domain-containing protein associated with the leukocyte NADPH oxidase. J Biol Chem 276, 18855–18862.

Muallem S, Kwiatkowska K, Xu X, Yin HL (1995). Actin filament disassembly is a sufficient final trigger for exocytosis in nonexcitable cells. J Cell Biol 128, 589–598.

Munafo DB, Johnson JL, Ellis BA, Rutschmann S, Beutler B, Catz SD (2007). Rab27a is a key component of the secretory machinery of azurophilic granules in granulocytes. Biochem J 402, 229–239.

Nakayama M, Goto TM, Sugimoto M, Nishimura T, Shinagawa T, Ohno S, Amano M, Kaibuchi K (2008). Rho-kinase phosphorylates PAR-3 and disrupts PAR complex formation. Dev Cell 14, 205–215.

Neeft M *et al.* (2005). Munc13–4 is an effector of Rab27a and controls secretion of lysosomes in hematopoietic cells. Mol Biol Cell 16, 731–741.

Pacquelet S, Johnson JL, Ellis BA, Brzezinska AA, Lane WS, Munafo DB, Catz SD (2007). Cross-talk between IRAK-4 and the NADPH oxidase. Biochem J 403, 451–461.

Pellegrin S, Mellor H (2008). Rho GTPase activation assays. Curr Protoc Cell Biol 8, Unit 14.

Pertz O, Hodgson L, Klemke RL, Hahn KM (2006). Spatiotemporal dynamics of RhoA activity in migrating cells. Nature 440, 1069–1072.

Pfeffer SR (2001). Rab GTPases: specifying and deciphering organelle identity and function. Trends Cell Biol 11, 487–491.

Price LS, Norman JC, Ridley AJ, Koffer A (1995). The small GTPases Rac and Rho as regulators of secretion in mast cells. Curr Biol 5, 68–73.

Raucher D, Stauffer T, Chen W, Shen K, Guo S, York JD, Sheetz MP, Meyer T (2000). Phosphatidylinositol 4,5-bisphosphate functions as a second messenger that regulates cytoskeleton-plasma membrane adhesion. Cell 100, 221–228.

Sasaki T, Shibasaki T, Beguin P, Nagashima K, Miyazaki M, Seino S (2005). Direct inhibition of the interaction between α-interaction domain and β-interaction domain of voltage-dependent Ca^{2+} channels by Gem. J Biol Chem 280, 9308–9312.

Stinchcombe JC, Barral DC, Mules EH, Booth S, Hume AN, Machesky LM, Seabra MC, Griffiths GM (2001). Rab27a is required for regulated secretion in cytotoxic T lymphocytes. J Cell Biol 152, 825–834.

Strom M, Hume AN, Tarafder AK, Barkagianni E, Seabra MC (2002). A family of Rab27-binding proteins. Melanophilin links Rab27a and myosin Va function in melanosome transport. J Biol Chem 277, 25423–25430.

Tolmachova T, Anders R, Stinchcombe J, Bossi G, Griffiths GM, Huxley C, Seabra MC (2004). A general role for Rab27a in secretory cells. Mol Biol Cell 15, 332–344.

Wang JS, Wang FB, Zhang QG, Shen ZZ, Shao ZM (2008). Enhanced expression of Rab27A gene by breast cancer cells promoting invasiveness and the metastasis potential by secretion of insulin-like growth factor-II. Mol Cancer Res 6, 372–382.

Wood SM *et al.* (2009). Different NK cell-activating receptors preferentially recruit Rab27a or Munc13–4 to perforin-containing granules for cytotoxicity. Blood 114, 4117–4127.

Yi Z, Yokota H, Torii S, Aoki T, Hosaka M, Zhao S, Takata K, Takeuchi T, Izumi T (2002). The Rab27a/granuphilin complex regulates the exocytosis of insulin-containing dense-core granules. Mol Cell Biol 22, 1858–1867.